2023-04-20

# A new equation to predict the shear strength of recycled aggregate concrete Z push-off specimens

Imjai, T



10.1016/j.cemconres.2023.107181
Cement and Concrete Research
Elsevier BV

# A new equation to predict the shear strength of recycled aggregate concrete Z push-off specimens

Accepted on April 12, 2023 by Cement and Concrete Research
ttps://doi.org/10.1016/j.cemconres.2023.107181

Author 1

- Thanongsak Imjai, PhD
- School of Engineering and Technology, Walailak University, Nakhonsithammarat, Thailand 80161
- 0000-0002-3220-7669

Author 2

- Fetih Kefyalew, MSc
- School of Engineering and Technology, Walailak University, Nakhonsithammarat, Thailand 80161
- 0000-0003-3600-7020

Author 3

- Pakjira Aosai, BSc
- School of Engineering and Technology, Walailak University, Nakhonsithammarat, Thailand 80161
- 0000-0003-0022-2626

Author 4

- Reyes Garcia, PhD
- School of Engineering, The University of Warwick, Coventry, UK CV4 7AL
- 0000-0002-6363-8859

Author 5

- Boksun Kim, PhD
- School of Engineering, Computing & Mathematics, University of Plymouth, Plymouth, PL4 8AA, UK
- 0000-0002-5890-3419

Author 6

- Hasan M Abdalla, PhD
- Faculty of Engineering, Civil Engineering Department, Sabratha University, Sabratha, Libya
- 0000-0003-0022-2626

Author 7

- Sudharshan N. Raman, PhD
- Civil Engineering Discipline, School of Engineering, Monash University Malaysia, Jalan Lagoon Selatan, 46200 Bandar Sunway, Selangor, Malaysia
- 0000-0003-4149-0141

Correspondence: thanongsak.im@wu.ac.th; Tel.: +66 (0) 7567 2378

**Abstract**

This article investigates the shear behaviour of Recycled Aggregate Concrete (RAC) Z push-off specimens. Fifteen specimens with different replacement levels of recycled concrete aggregate (0%, 25%, 50%, 75% and 100%) were tested. It is shown that a 100% RCA replacement level reduces shear strength by 17.3%. The shear behaviour of the specimens was further analysed using nonlinear finite element analysis (FEA). The results show that the shear strength results from the FEA and Digital Image Correlation measurements agree (within 5%) with the experimental results. This study proposes a new semi-empirical equation to calculate the shear strength of specimens with different RAC replacement levels. The new equation adopts a fracture mechanics approach, and it explicitly considers the shear deformation and crack opening. Compared to existing models, the new equation fits better the experimental data in this study, as well as test results from an extensive database obtained from the literature.

**Keywords:** *Recycled aggregate concrete; Z push off specimen; shear plane; shear strength; fracture behaviour; Mode II stress intensity factor; Finite element analysis.*

## 1. Introduction

In recent years, rapid population growth and urbanisation have led to an extensive renovation of the old building stock in Southeast Asia. This has created a steady stream of demolished concrete which, if properly recovered and sorted, can be used as Recycled Concrete Aggregate (RCA) in new Recycled Aggregate Concrete (RAC). The replacement of natural aggregates with RCAs impacts positively on the environment and promotes a more efficient use of resources. However, RCAs are usually weaker than natural aggregates as the former are more porous and contain residues of old mortar. As a result, RACs are seldom used in structural applications as the resistance mechanisms of concrete can be affected by the inferior properties of RCAs.

Recent research by the authors [1, 2] have identified that, whilst the compressive and flexural behaviour of RAC elements has been extensively examined, less research has focused on their shear behaviour [3-12]. Xiao et al. [13] reported results on the shear-transfer behaviour between natural aggregate concrete (NAC) and RAC pre-cracked Z push-off specimens. The results indicated that the mechanism and process of shear transmission across cracks in RAC are generally similar to those observed in NAC. However, for RCA replacement ratios above 30%, the shear transfer strength of RAC reduced by 15% or more. Additionally, the design formulae for NAC included in ACI 318 were found suitable to conservatively predict the shear transfer strength of RAC. Rahal and Hassan [14] observed a significant reduction in shear strength of their initially uncracked push-off specimens due to the partial replacement of natural aggregate concrete (NCA) with RCA. Nevertheless, they concluded that 100% replacement of aggregates with recycled ones had a negligible effect on shear strength. The inconsistency of experimental results (especially at high levels of aggregate replacement) and limited amount of data make standardisation difficult [15]. Therefore, more experimental data is still necessary. The lack of data is also reflected in current guidelines [16,17] which limit the maximum replacement of coarse RCA to 20% in new structural RAC elements. To the authors' knowledge, no shear-strength predictive model exists even though comparisons of the measured strengths have been made with the current ACI 318 shear friction predictive equation for plain concrete, which only depends on the compressive strength [18].

The shear behaviour of concrete elements is a complex phenomenon [19]. This is because the shear transfer mechanism mobilised at a shear crack depends heavily on aggregate interlock and dowel action [20], both of which are affected by the surrounding stress conditions. In this phenomenon, the dilatancy of the shear cracking is influenced by the roughness of the two contact faces of a crack. When the dilatancy of the fracture increases, the shear stiffness along the cracks reduces [21]. For transversal reinforcement of push off specimen the crack behaviour for slip displacements up to 10 mm is possible, this threshold allows micro and macro roughness [22,23]. Shear may have to be transferred across planes of existing or potential cracks or interfaces between elements of a beam such as flanges and webs or across interfaces between concretes placed at different times [24]. In such cases, shear failure may involve sliding along a plane of weakness rather than the diagonal tension failure which is more common in a beam-like element under one-way shear [25]. In general, the shear strength in Z push-off specimens developed along the plane on which sliding occurs consists of i) frictional resistance, ii) resistance to shearing off the aggregate protrusions on the irregular crack surface (aggregate interlock), and iii) resistance developed in the transverse reinforcement bridging the plane. The aforesaid shear resisting mechanisms are known as interface shear or shear friction [26].

Past research has also proposed various models describing the shear transfer mechanism in push-off tests. Liu et al [27] investigated the shear-transfer mechanism of a shear interface with transverse reinforcement between a precast girder made of high-strength concrete. Walraven and Reinhardt [28] carried out different shear tests on concrete specimens and proposed micro-models for shear transfer mechanisms. Based on a series of Z-push off results, they proposed an empirical model (Eq. (1)) that included shear displacement, normal stress, and crack opening along the shear plane:

$$\tau_{agg} = -\frac{f_c}{30} + (1.8w_s^{-0.80} + (0.234w_s^{-0.707} - 0.20)f_c))\Delta_y \tag{1}$$

where $\tau_{agg}$ is the concrete shear strength (or stress) due to aggregate interlock; $f_c$ is the concrete compressive strength; and $w_s$ and $\Delta_y$ are the crack width and the slip at the shear plane, respectively.

It should be noted that Eq. (1) was derived empirically based on limited experimental data. The equation also depends heavily on the type of concrete (i.e. its compressive strength) and the shear deformation due to aggregate interlocking mechanism. Moreover, recent experimental evidence confirmed that the properties and amount of RCA replacement play an important role in the shear strength due to the amount of residual mortar [1,2, 10-12]. Whilst it is difficult to determine the amount of residual mortar in a mix design, the amount of RCA replacement in a mix is always known. Thus, the shear strength of plain RAC elements should not only depend on the concrete compressive strength, but also on the amount of RCA replacement. To address this issue, Li and Maekawa [29] proposed calculating $\tau_{agg}$ across a crack of RAC using Eq. (2):

$$\tau_{agg} = 3.83 f_c^{0.33} \left(\frac{R}{1 + R^2}\right) \tag{2}$$

where $R$ is the percentage of recycled concrete aggregate replacement, and $f_c$ is the compressive strength. According to Eq. (2), the shear strength only depends on the concrete strength and RCA replacement level. However, at the crack across the shear plane and the shear deformation (crack width and slips) plays an important role in the aggregate interlocking phenomenon and, as a result, they heavily affect the shear transfer stress along the crack plane. However, experimental evidence has confirmed that the RCA replacement level and shear deformation along the crack plane can significantly affect the concrete shear strength, both of which are not included in Eqs. (1) and (2) as limited research exists on the subject. Therefore, there is a need to develop a more accurate and meaningful shear models for plain RAC element to include both RCA replacement level and shear deformation along the crack plane.

This study investigates experimentally and numerically the shear failure mechanics of RAC. To achieve this, fifteen push-off specimens with initially uncracked shear planes were tested. The parameters varied in the push-off tests were the replacement level of recycled aggregates (0, 25, 50, 75, or 100%), and the concrete strength. Shear deformation is further investigated using digital image correlation (DIC). A nonlinear finite element analysis (FEA) is also carried out to investigate the shear deformation along the shear plane of the specimens. Based on the test results, a new semi-empirical-based model for shear transfer stress in plain concrete with different RCA replacement levels is proposed. The model adopts a fracture mechanics approach, and it explicitly includes the shear displacement and crack opening. This investigation is expected to promote the safe structural use of RAC in shear-critical elements.

## 2. Experimental programme

### 2.1 Details of Z push-off specimen

Fifteen Z-shaped specimens were cast with RAC, according to the dimensions and reinforcement details shown in Fig 1a. The dimensions of the specimens (200mm wide, 500mm tall and 100mm thick) were similar to those adopted in a previous study [13]. The specimens were reinforced longitudinally with four 12mm bars, and transversally with square stirrups of 6mm at 50mm centres. To allow the concrete to carry all the shear stresses during the test, no transverse reinforcing bars were provided across the 100×200mm crack plane. Three control specimens were cast with NAC. The other twelve specimens were cast with RAC containing four different levels of RCA replacement: 25%, 50%, 75% or 100%. Each group had three identical samples. The specimens were identified based on the percentage of RCA replacement (RCA0=control, RCA25, RCA50, RCA75 and RCA100), followed by a Roman number that designated the number sample within the percentage group.

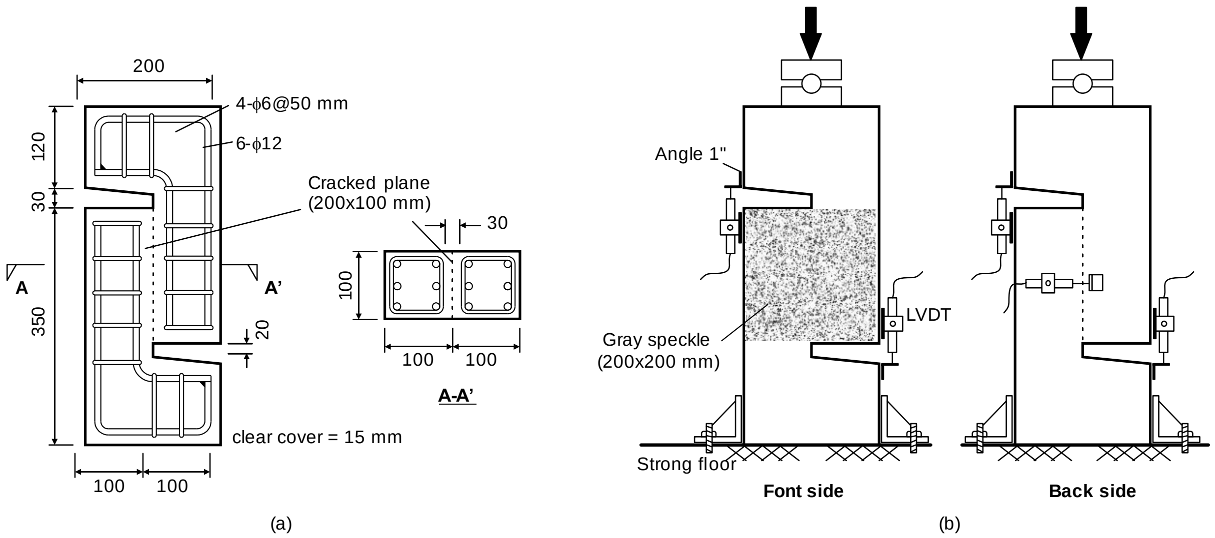


**Fig. 1.** (a) Geometry and reinforcement details of Z push-off specimens, and (b) schematic test setup and instrumentation (units: mm).

### 2.2 Concrete mix properties

Ordinary Portland Cement (OPC) Type I was used to cast the specimens. The RCA was sourced from concrete cylinders (150×300mm) from a batch used in a local construction. The average strength of the original cylinders was 45 MPa. Coarse recycled aggregate of sizes of 12mm (RC#1) and 19mm (RC#2) were produced (see Fig. 2) using a custom-made crushing machine. Fine RCA was collected using a tray under the machine, and subsequently sieved to the match the fine aggregate used for normal concrete. Fig. 2a shows the RCA, whereas Fig. 2b presents the particle size distribution of the natural aggregate and RCA. The physical and mechanical properties of the aggregates are shown in Table 1.

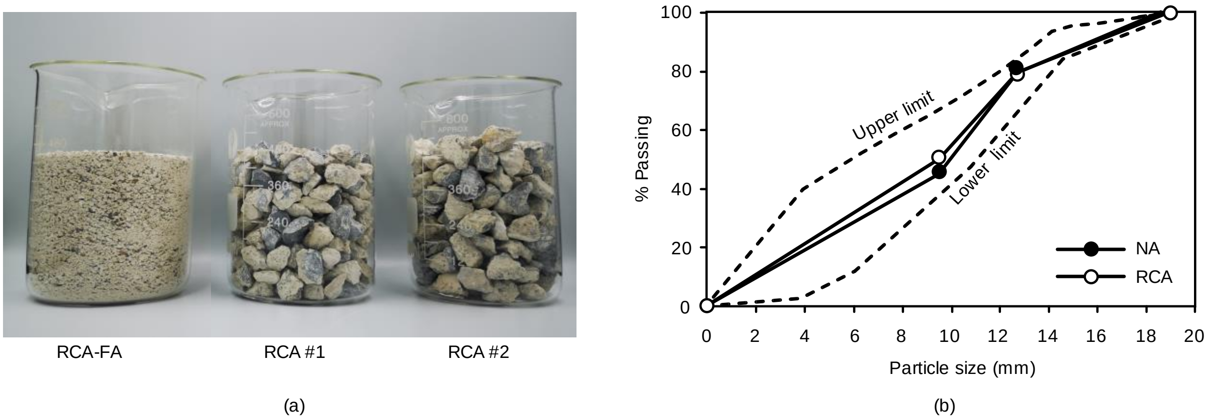


**Fig. 2.** (a) Coarse and fine RCA, and (b) size distribution of natural aggregates and RCA.

**Table 1.** Physical and mechanical properties of coarse and fine aggregates.

| Properties | NC | RCA#2 | RCA#1 | N-FA | RCA-FA |
|---|---|---|---|---|---|
| Bulk Specific Gravity | 2.71 | 2.43 | 2.51 | 2.60 | 2.77 |
| Unit Weight (kg/m3) | 1730 | 1397 | 1425 | 1550 | 1400 |
| Water Absorption (%) | 0.28 | 4.59 | 5.13 | 1.05 | 2.65 |
| Moisture (%) | 0.61 | 2.24 | 2.14 | 1.35 | 2.42 |
| Fineness Modulus | - | - | - | 2.7 | 1.8 |
| Max. size (mm) | 19.1 | 18.6 | 9.8 | 4.76 | 4.70 |
| Impact value (%) | 10.15 | 13.4 | 12.5 | - | - |
| Crushing value (%) | 21.77 | 23.12 | 20.12 | - | - |
| Residual mortar (%) | - | 32.5 | 30.2 | - | 32.5 |

NC=natural coarse, RCA#1=coarse RCA 12 mm, RCA#2=coarse RCA 19 mm, N-FA=natural fine, RCA-FA=fine RCA

As shown in Table 1, superplasticiser (SP) was also utilised to increase the workability of the mixes. Slump cone tests were performed to measure the consistency of the fresh mixes. Table 2 shows the final mix proportions used to cast the different concretes. Five mixes were designed with a water–cement ratio of 0.53 with a target compressive strength of 30 MPa and a slump of 90 mm. The mix proportions of the mixes are shown in Table 2.

**Table 2.** Concrete mix proportion containing different RAC replacement (units: kg/m$^3$)

| Mix | Cement | NC | RC | NF | RF | Water | Superplasticiser | Slump (mm) |
|---|---|---|---|---|---|---|---|---|
| RCA0% | 357 | 1069 | - | 719 | - | 190 | 1.07 | 90 |
| RCA25% | 357 | 802 | 267 | 180 | 540 | 190 | 1.07 | 85 |
| RCA50% | 357 | 535 | 535 | 360 | 360 | 190 | 1.07 | 85 |
| RCA75% | 357 | 267 | 802 | 540 | 180 | 190 | 1.07 | 84 |
| RCA100% | 357 | - | 1069 | - | 719 | 190 | 1.07 | 80 |

The mechanical properties of NCA and RAC mixes are shown in Table 3. The mean compressive strength was obtained from six 150×300mm cylinders ($f_{cyl}$) and fifteen 150mm cubes ($f_{cub}$) according to BS EN 12390-3 [30]. The indirect tensile splitting strength ($f_t$) was determined from tests on six 150×300mm cylinders according to BS EN 12390-6 [31]. The flexural strength ($f_b$) was obtained from four-point bending tests on six prisms of 100×100×500mm according to BS EN 12390-5 [32]. All the cubes, cylinders and prisms were cast from the same batch and cured together with the slabs until testing. As expected, the compressive and tensile strengths reduced as the amount of RCA replacement increased. The corresponding densities for NA, 25%RCA, 50%RCA, 75%RCA and 100%RCA calculated according to Eurocode 2 [33] were 2400 kg/m$^3$, 2365.8 kg/m$^3$, 2331.5 kg/m$^3$, 2297.3 kg/m$^3$and 2263 kg/m$^3$, respectively.

**Table 3.** Mechanical properties concrete mixes at 28 days.

| Concrete mix series | $f_{cy}$ (MPa) | $f_{cu}$ (MPa) | $f_t$ (MPa) | $f_b$ (MPa) |
|---|---|---|---|---|
| RCA0% | 35.2 | 39.2 | 4.0 | 5.4 |
| RCA25% | 32.4 | 37.8 | 3.8 | 5.0 |
| RCA50% | 28.9 | 37.9 | 3.4 | 4.8 |
| RCA75% | 26.5 | 36.6 | 2.7 | 4.0 |
| RCA100% | 24.8 | 32.6 | 2.5 | 3.8 |

## 2.3 Digital Image Correlation

Past research shows that DIC is very effective at measuring shear deformations of concrete samples with an error of 5-15% [34-36], based on the surface deformation processing principle. In this study, a bespoke DIC software (WU-DIC v2021 [37]) developed in Python was used to measure shear deformations of the Z push-off specimens. Fig. 3a shows a Z push-off specimen with a typical DIC speckle pattern, whereas Fig. 3b shows the measuring kit. The tracking of speckles was performed using a Canon EOS 5D Mark IV camera configured at a maximum resolution of 4480×6720 pixels. The camera was mounted on on a tripod located at 500mm from the object (FOV). A Canon EF 50mm lens with a minimum focus distance of 0.21m and a maximum focus distance of 0.35 m was used. The FOV was illuminated by eight LED lamps of 300 W with a brightness of 60000 lux to control the brightness level of the sample surface. Table 4 shows the parameters used in the DIC analysis.

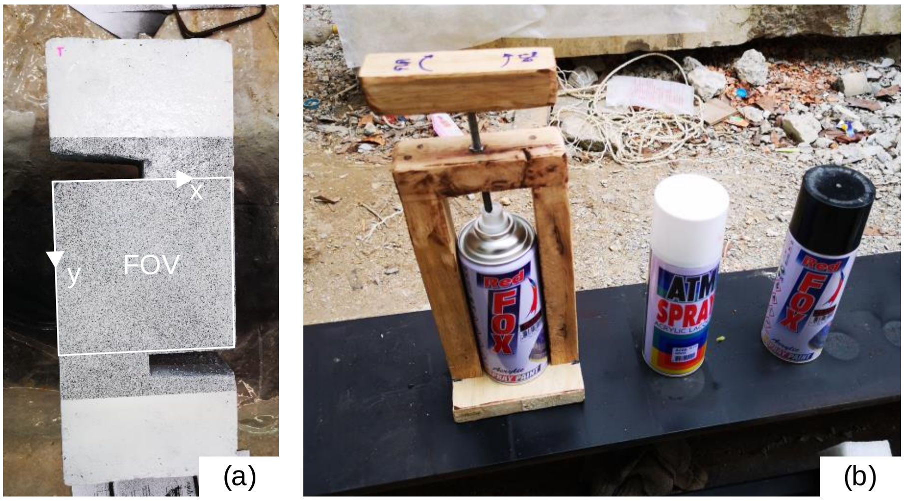


**Fig.3.** (a) Typical view of grey speckle of Z-push off specimens, and (b) DIC grey speckle kit.

**Table 4.** DIC analysis parameters.

| DIC parameters | value | Unit |
|---|---|---|
| Focal length | 50 | Mm |
| FOV | 200×200 | Mm |
| Recording resolution | 4480×6720 | Pixel |
| Objection-camera distance | 500 | Mm |
| Speckle dimension | 4.27 | Pixels |
| Object speckle dimension | 0.35 | mm |
| Facet size | 19×19 | pixels |
| Recording trigger | 0.5 | sec |

### 2.4 Instrumentation and testing procedure

The specimens were positioned vertically on a strong floor, with the base being supported by steel supports as shown in Fig. 4. The specimens were loaded using a 100kN-capacity hydraulic jack. A hinge support was placed between the jack and the specimen. A guide roller was also used to prevent out of plane movement of the specimen during the test. To measure shear displacements, two displacement transducers were mounted vertically at the Z notches. Another horizontal transducer (near the centre of the specimen) monitored the crack opening during the test. The loading protocol was as follows: prior to reaching 70% of the estimated ultimate shear load $P_u$, a loading step $P_u/10$ was used to increase the load by ten percent. Once the load was between $0.7P_u$ and $0.9P_u$, the loading step reduced to $P_u/20$. After reaching 0.9Pu, the test was controlled using the LVDT displacement at a rate of 0.02 mm/min. The tests were terminated when shear failure of the specimens occurred.

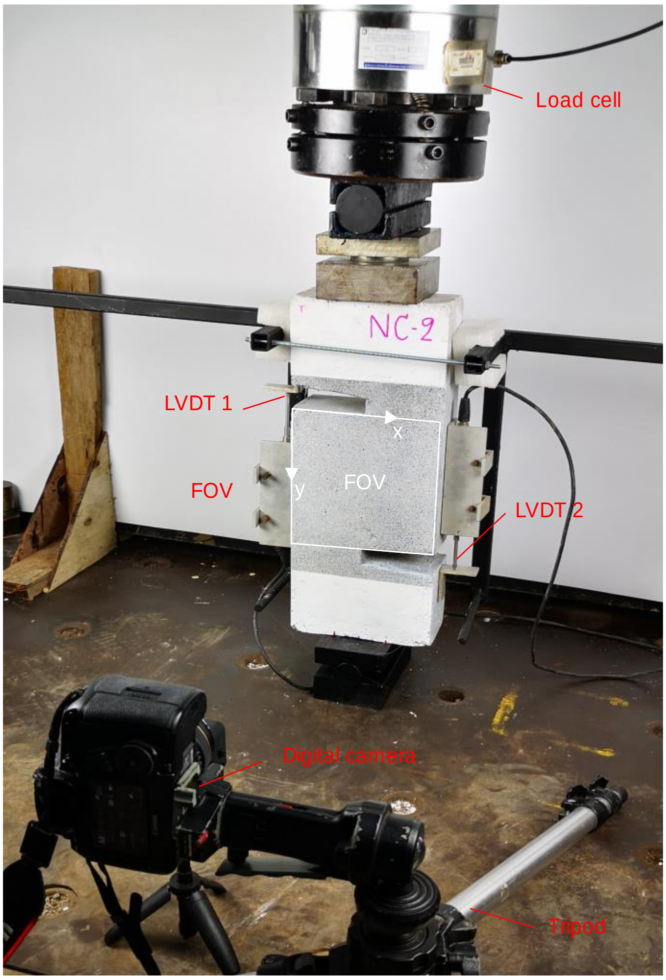


**Fig. 4.** Instrumentation and loading arrangement.

# 3. Test results and discussion

## 3.1 Failure mode

Table 5 summarises the main results from the tests, including ultimate shear load ($P_u$), ultimate shear stress ($\tau_u = \frac{P_u}{A_c}$), mean crack width ($w_c$), and vertical slip ($\Delta_y$) at $P_u$. It can be seen from Table 5 that the shear stress and crack width range between 4.91-5.38 MPa and 0.23-0.61mm respectively. The results in Table 5 indicate that an increase in the percentage of RCA from 25%, 50%, 75% to 100%

decreases the corresponding shear strength (ratios 1.01, 1.02, 1.05 and 1.08 respectively) compared with specimen RCA0. Fig. 5 shows the failure of a typical Z push-off specimen.

**Table 5**. Summary of results from Z push-off tests

| Concrete mix series | Specimen | $f_c$ (MPa) | $P_u$ (kN) | $\tau_u$ (MPa) | $w_c$ (mm) | $\Delta_y$ (mm) |
|---|---|---|---|---|---|---|
| RCA0% (control) | RCA0%-I | 35.2 | 107.65 | 5.38 | 0.43 | 0.74 |
| | RCA0%-II | | 106.83 | 5.34 | 0.32 | 0.81 |
| | RCA0%-III | | 106.20 | 5.31 | 0.38 | 0.78 |
| RCA25% | RCA25%-I | 32.4 | 106.45 | 5.32 | 0.44 | 0.91 |
| | RCA25%-II | | 105.96 | 5.29 | 0.61 | 0.66 |
| | RCA25%-III | | 105.55 | 5.28 | 0.32 | 0.86 |
| RCA50% | RCA50%-I | 28.9 | 105.45 | 5.27 | 0.47 | 0.92 |
| | RCA50%-II | | 104.69 | 5.23 | 0.57 | 0.82 |
| | RCA50%-III | | 105.30 | 5.26 | 0.56 | 0.91 |
| RCA75% | RCA75%-I | 26.5 | 102.84 | 5.14 | 0.48 | 0.95 |
| | RCA75%-II | | 101.78 | 5.09 | 0.41 | 0.84 |
| | RCA75%-III | | 102.21 | 5.11 | 0.47 | 0.56 |
| RCA100% | RCA100%-I | 24.8 | 98.37 | 4.91 | 0.56 | 1.11 |
| | RCA100%-II | | 99.20 | 4.96 | 0.23 | 0.96 |
| | RCA100%-III | | 100.03 | 5.00 | 0.57 | 1.24 |

Note: $f_c$=compressive strength, $P_u$=compressive load, $\tau_u$=shear stress, $w_c$=crack width and $\Delta_y$=slip

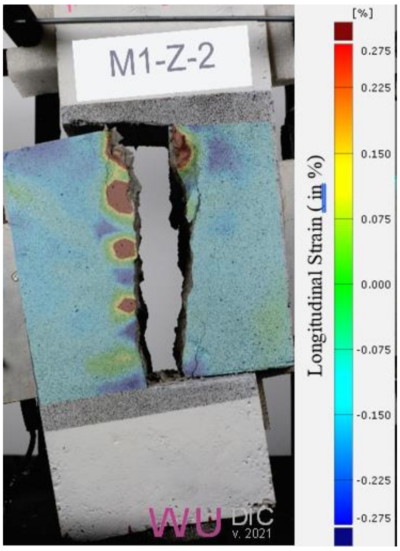


**Fig. 5.** Failure of typical Z push-off specimen (specimen RCA0%).

## 3.2 Shear stress vs displacement curves

Fig. 6 presents the shear stress vs displacement response for the tested specimens. In this figure, the crack width was measured by horizontal displacement transducers, whereas the shear displacement was monitored by the vertical displacement transducer. The results indicate that, at the start of loading, the crack separation changes very little. Before the ultimate shear stress is reached, the crack has nearly the same width along the specimen depth. It can also be noted that the crack width curves for the NAC specimens and for the RAC specimens share the same features, regardless of the different amounts of RCA used in the latter. The curves are convex before the ultimate shear stress is reached. After that, an inflection point appears, followed by quick growth of both crack width and shear displacement and the final failure.

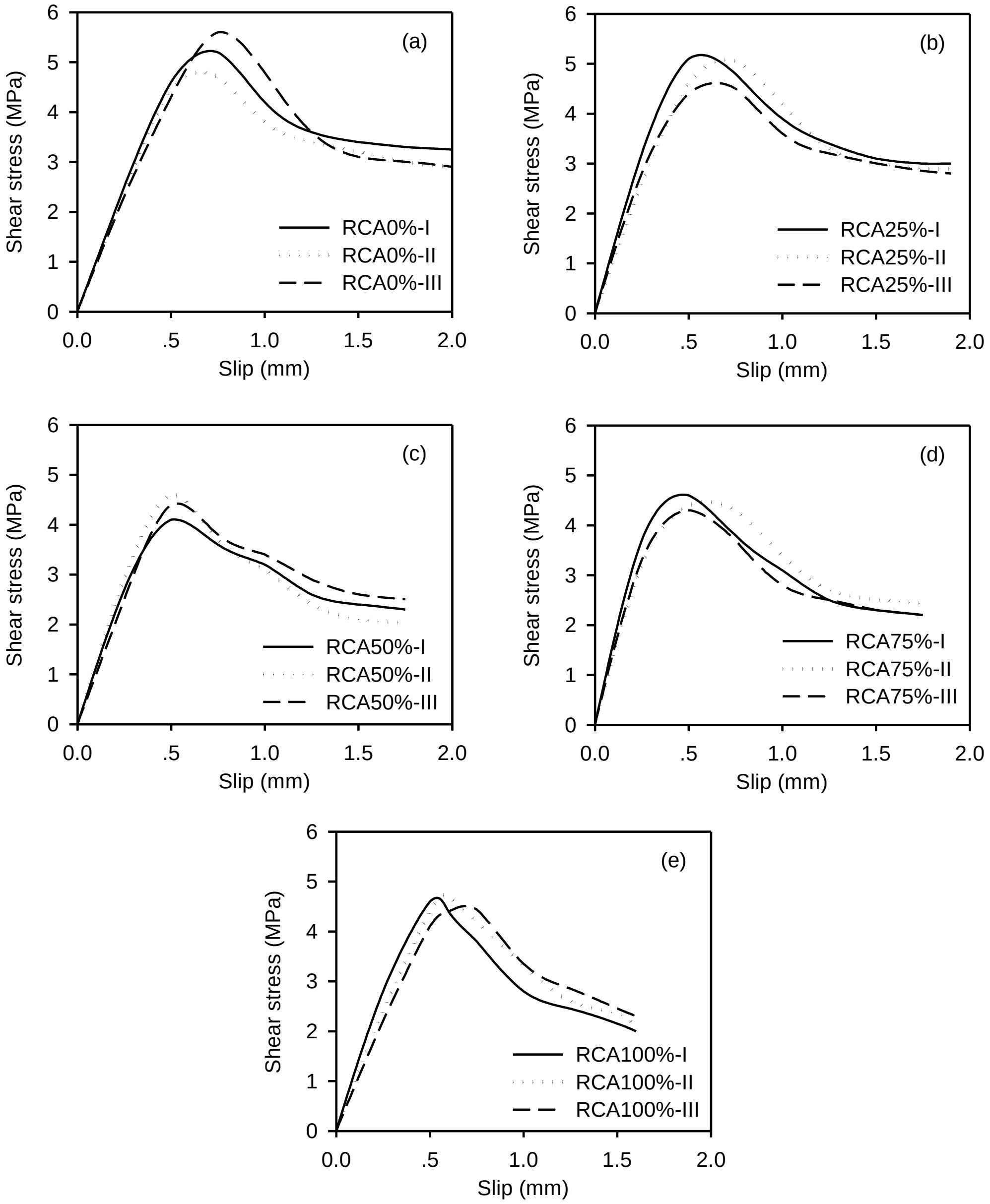

**Fig. 6.** Experimental shear stress vs slip curves for specimens: a) normal concrete (NC), b) 25% RCA replacement, c) b) 50% RCA replacement, d) 75% RCA replacement, and e) 100% RCA replacement

### 3.3 Crack width and slip measurements

Fig. 7 shows the relationship between shear slip ($\Delta_y$) and crack width ($w_c$) for specimens with different RCA contents. the specimens were positioned vertically and supported by a fixed bearing. The crack separation and was measured at the shear plane positions by horizontal displacement transducers, and the sliding was measured by two displacement transducers were mounted vertically at the Z notches near the specimen's center on at the shear plane position. It is shown that, in the initial period of loading, the crack width hardly changes. Before the ultimate shear load is reached, the crack has nearly the same width along the specimen depth. Fig. 7 also indicates that the crack separation curves of all specimens share the same features. They are convex before the ultimate shear stress is reached. After that an inflection point appears, followed by quick growth of both crack width and shear slip and final failure.

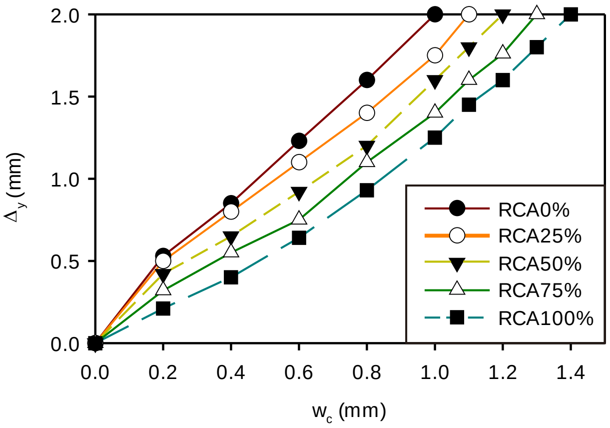


**Fig. 7.** Relationship between crack width and slip for different specimens

### 3.4 Effect of concrete compressive strength

Fig. 8 presents the shear stress vs compressive strength response of the tested specimens. The results in this figure show that the shear strength increases with increasing compressive strength. This is due to the increase in initial shear transfer stiffness as the compressive strength also increases. It can be seen from Fig. 8 that the ultimate shear stress of the RCA specimens tends to improve with the increase of concrete strength.

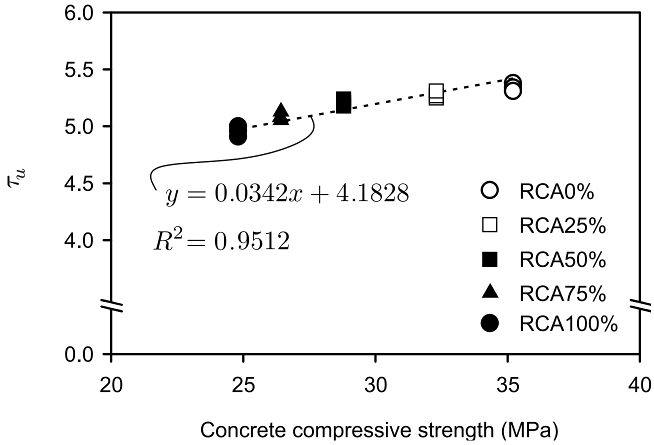


**Fig. 8.** Relationship between concrete shear strength and concrete strength for groups of specimens

## 3.5 Effect of recycled aggregate replacement level

Fig. 9 shows the variation of shear stress with the RCA replacement level. The results show that the shear stress decreases with increasing RCA replacement levels. However, in all cases the reduction in shear stress was minor (less than 10%). This is believed to be due to an internal curing action of the saturated surface dry recycled aggregate particles (which strengthened the concrete matrix) and thus increased the shear strength.

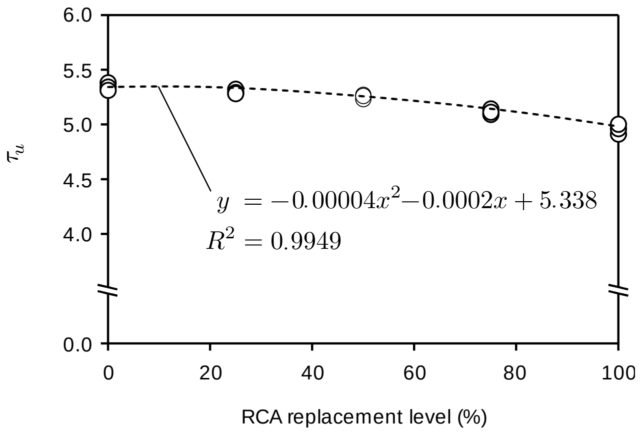


**Fig. 9.** Effect of RCA replacement on concrete shear stress.

Fig. 10 shows the calculated shear stresses normalised with reference to their respective cylinder compressive strengths as a function of the RCA replacement levels. The shear strength of the specimens is attributed to cohesion and aggregate interlock, and it is seen to be significantly dependent of the RCA replacement levels.

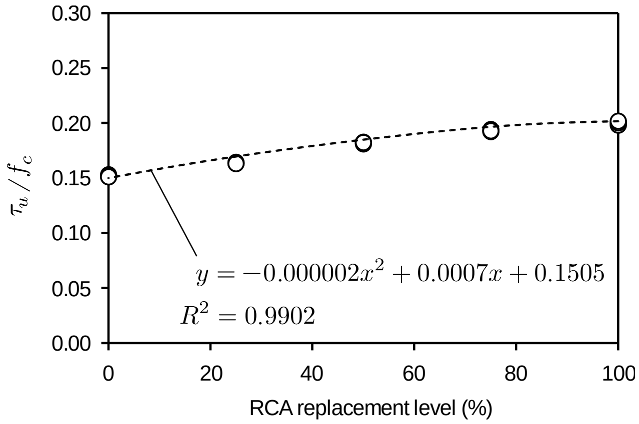


**Fig. 10.** Effects of RCA replacement levels on the $\tau_u/f_c$ ratio

## 4. Numerical study on shear deformations

The commercial finite element (FE) package ANSYS was used to numerically predict the shear behaviour of the Z push-off specimens and to explore the influence of percentage of RAC on the response. The mean moduli of elasticity of NA, 25%RCA, 50%RCA, 75%RCA and 100%RCA was calculated using Eurocode 2 [33] and were 33.2 GPa, 32.6 GPa, 32.1 GPa, 31.5 GPa and 30.1 GPa, respectively. The size independent fracture energy ($G_f$) from the same mix concrete design was obtained from three-point bending tests [38] and calculated according to the RILEM recommendations [39]. The shear stress vs displacement relationship of five specimens with different RCA percentages were then compared with the results given by the FE model. Eight-node hexahedron solid elements were adopted to model the concrete. The element size was 4 mm, as determined by a convergence study. The number of elements and nodes were 62,500 and 83,800 respectively. Following the FE model's validation, the plot of the shear stress vs. slip relationship was examined using common simulation and experimental findings as shown in Fig. 13. A regression analysis was then carried out for evaluating the expressions of the ultimate shear stress and direct shear stress vs deflection curves.

Fig. 11 compares the crack patterns obtained from the FEA and DIC for a specimen with RCA replacement level of 100%. Overall, the predicted crack patterns obtained from both FE and DIC agreed very well with the experimental observations.

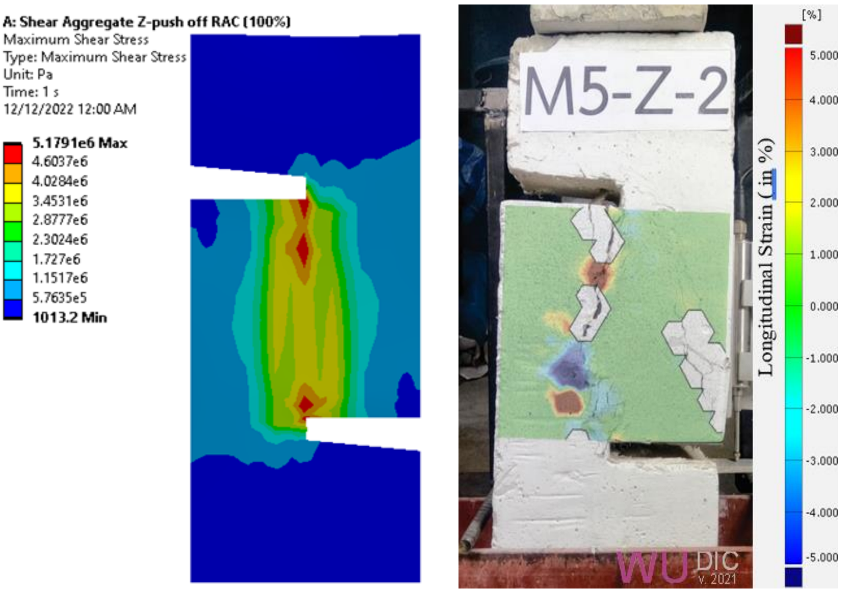


**Fig. 11.** FEM result of shear stress for 100% RCA replacement level

# 5. A new shear strength model for RAC

## 5.1 Shear transfer mechanism

The analysis of shear transfer in the push-off specimens is based on Airy's stress function and Mohr's circle theory. A Mode II type of fracture (Fig. 12a) [40] is assumed to occur in the specimens (Fig. 12b), with a shear sliding mechanism as shown in Fig. 12c. The stresses acting on a small element of concrete lying in a shear plane are shown in Fig. 12d. The objective of the analysis is to predict the shear strength acting on the element that will lead to failure of concrete in the shear plane. Using Mohr's circle, a relationship between shear stress and normal stress is constructed in an originally uncracked push-off specimen. In Fig. 12d, $\sigma_x$ is the normal stress on the shear plane brought on by the transverse plain, $\sigma_y$ is the normal stress brought on by the applied load, and $\tau_{xy}$ is the shear stress.

In the early stages of loading history (i.e. when the concrete in the shear plane is in uncracked), the stresses in the transverse plain are negligible. Diagonal cracks develop along the shear interface as the applied load increases, and these cracks create an angle θ (Fig. 12d). This occurs when the principal tensile stress in the concrete surpasses its tensile capacity. Due to applied load, the fracture develops on the specimen shear plane as shown in Fig. 12b. This results in the crack surface sliding relative to each other (Fig. 12c), and this sliding mode is Mode II. This mode of fracture defined by Westgarden function and transferred to shear based on Mohr's circle principal stress (Fig 12d)

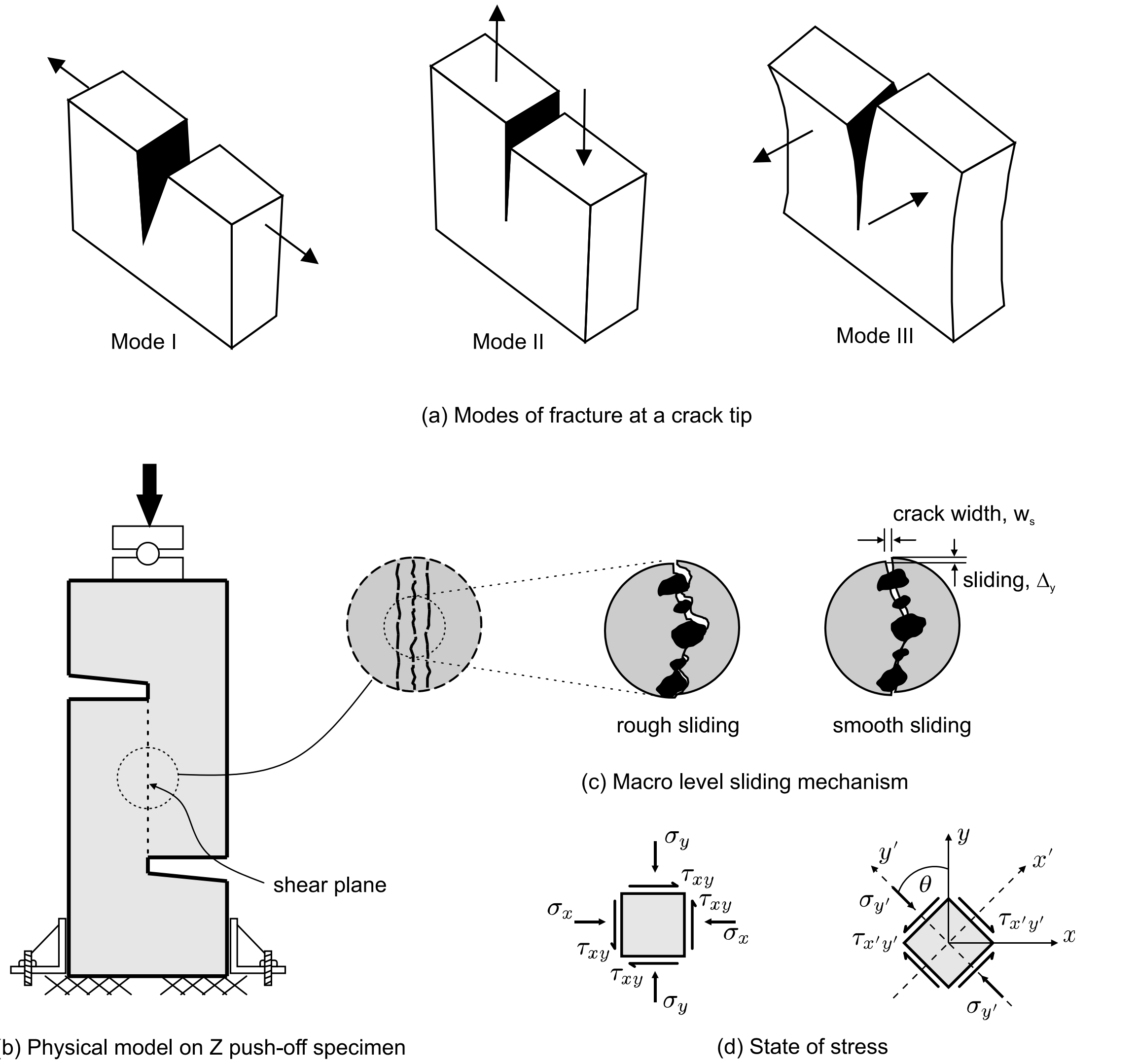


**Fig.12.** (a) Three modes of deformation at a crack tip, (b) physical model of Z push-off specimens, (c) shear transfer mechanism along the shear plane, (d) state of stresses in a particle of concrete.

To understand the interface cracking mechanism, a small (rotated) concrete element in a diagonal strut is also considered (Fig. 12d). The stresses acting on this element comprise of $\sigma_{y'}$ acting along the direction of diagonal cracks and shear stresses, and $\tau_{x'y'}$ oriented normal to the direction of diagonal cracks. As failure approaches, the diagonal cracks widen, the faces of the crack become unstressed free surfaces, and thus $\sigma_{x'}$ can be considered as zero. The objective of this analysis is to obtain values of $\tau_{x'y'}$ that correspond to cracking along the interface shear plane in the context of a predefined interface cracking envelope. Airy's stress function for Mode II of fracture [41-43] (Fig. 12a) is expressed in polar coordinates by Eq. (3):

$$\phi_{II} = -\mathrm{yRe}|Z| \tag{3}$$

where the real part of $Z$ represents Westergarden's function [44], which for Mode II of fracture can be defined as follows:

$$Z_{(z)} = \frac{\tau_o \times z}{\sqrt{z^2 - a^2}} \tag{4}$$

where $\tau_o$ is the initial shear, and $a$ is the length of shear surface in the specimen.

Airy's stress function transformation to shear can be derived from Mohr's circle [45]:

$$\begin{aligned} \sigma_{xx} &= \frac{\partial^2 \phi}{\partial_{y^2}} = 2\mathrm{Im}Z_{II} + Y\mathrm{Re}Z'_{II} \\ \sigma_{yy} &= \frac{\partial^2 \phi}{\partial_{x^2}} = -Y\mathrm{Re}Z'_{II} \\ \tau_{xy} &= \frac{-\partial^2 \phi}{\partial_x \partial_y} = \mathrm{Re}/Z_{II}/-Y \times \mathrm{Im}/Z'_{II}/ \end{aligned} \tag{5}$$

By substituting the real and imaginary parts of Eq. (4) and its derivative into Eq. (5), and by adopting Euler's theorem $Z = re^{i\theta} = r(\cos\theta + i \times \sin\theta)$, Eq. (6) can be obtained:

$$\begin{Bmatrix} \sigma_x \\ \sigma_y \\ \tau_{xy} \end{Bmatrix} = \frac{K_{II}}{\sqrt{2\pi r}} \sin\frac{\theta}{2} \begin{Bmatrix} -2 - \cos\frac{\theta}{2}\cos\frac{3\theta}{2} \\ \cos\frac{\theta}{2}\cos\frac{3\theta}{2} \\ \cot\frac{\theta}{2}\left(1 - \sin\frac{\theta}{2} - \sin\frac{3\theta}{2}\right) \end{Bmatrix} \tag{6}$$

The shear stress after sliding $\tau_{x'y'}$ is shown in Eq. (7), whereas Eq. (8) shows the transferred shear stress by substituting Eq. (6) into Eq. (7):

$$\tau_{x'y'} = -\left(\frac{\sigma_x - \sigma_y}{2}\right) sin2\theta + \tau_{xy}\cos 2\theta \tag{7}$$

$$\tau_{x'y'} = \frac{K_{II}}{\sqrt{2\pi r}}\left(\frac{\sin\theta}{2} sin2\theta \left(1 + \frac{\cos\theta}{2}\frac{\cos 3\theta}{2}\right) + \frac{\cos\theta}{2}\cos 2\theta\left(1 - \frac{\sin\theta}{2} - \frac{\sin 3\theta}{2}\right)\right) \tag{8}$$

The stress intensity factor [43] for Mode II can be defined as $K_{II} = Y \times \tau_o\sqrt{\pi \times a}$, where $Y= F(2a/L)$ is a geometry factor related to specific crack geometry. Ko and Kemeny [44] suggested the value of $f\left(\frac{2a}{L}\right) = 0.15 + 0.54\left(\frac{2a}{b}\right)$ based on finite element analysis using the displacement extrapolation method for a Mode II of fracture.

Fig. 10 shows that a regression analysis yields the relationship between shear stress and RCA replacement level as $\tau = (-2 \times 10^{-6}R^2 + 7 \times 10^{-4}R + 0.1505)f_c$, where $R$=RCA replacement level, $f_c$ =compressive strength. The Mode II stress intensity factor in terms of this parameter results in $K_{II} = (-0.7272 \times 10^{-6}R^2 + 2.5452 \times 10^{-4}R + 0.05474)f_c$.

The parameter $r$ in Eq. (8) can be obtained using Pythagoras theorem as $r^2 = w^2 + \Delta^2 + a^2 - 2a\Delta$, where, $w$=crack width, $\Delta$ =slip and $a$ =distance from centre of shear plane to tip. Using trigonometric identity substitution, Eq. (9) expresses the shear strength as a function of the RCA replacement level and shear deformation along the cracked plane:

$$\tau_{x'y'} = \left[\frac{(-0.7272 \times 10^{-6}R^2 + 2.5452 \times 10^{-4}R + 0.05474)f_c}{\sqrt{2\pi\sqrt{w^2 + \Delta^2 + a^2 - 2a\Delta}}}\right] \times \left[\begin{array}{l}\sqrt{\frac{1-\cos\theta}{2}} \times \sin\theta\cos\theta(2+\cos\theta+\cos^2\theta) + \sqrt{\frac{1+\cos\theta}{2}}\sin^2\theta\cos\theta(2\cos\theta - 1) \\ -\sqrt{\frac{1+\cos\theta}{2}}\sqrt{\frac{1-\cos\theta}{2}\sin^2\theta\cos^2\theta(\cos\theta-1) - \frac{1}{2}\cos^2\theta\sin^3\theta(1+\cos\theta)}\end{array}\right] \tag{9}$$

It should be noted that the shear stress function obtained by boundary condition at $\theta$ =0, by substituting the parameters after fracture and the constants (geometry of specimen) to the governing Eq. (9) the angle at the shear plane leads to $\theta$ =11°.

Finally, by substituting the geometry of the Z push-off specimens tested in this study ( $a$ =0.1m and $b$ =0.1m), the (aggregate) shear strength can be expressed as:

$$\tau_{agg} = \left[\frac{-0.64 \times 10^{-6} R^2 + 0.223 \times 10^{-3} R + 0.04796}{\sqrt[4]{(w^2 + \Delta^2 - 0.2\Delta + 0.01)}}\right] \times f_c \tag{10}$$

where $\tau_{agg}$ is the shear transfer stress in plain concrete; and the rest of the variables are as defined before.

It is noted that the proposed semi-empirical Eq. (10) adopts a Mode II stress intensity factor and data from a regression analysis, where the latter depend on both concrete compressive strength and RCA replacement levels. Since the scope of the present study is limited to the identical geometry of Z push-off specimens and all the specimens had the same geometry to minimize the “size effect” as this can be one of an interesting topic when studying shear concrete strength with different specimen’s size. i.e the behavior would behave more brittle when larger specimens are used (compare to smaller specimens that more ductile behavior is expecting). The proposed model can be later modified to include the size effect i.e. shear span ratio/beam depth. However, the new equation explicitly considers the shear deformation along the cracked plane (i.e. crack width and slip). It is worth mentioning that the RCAs used in this study were obtained from a known source (same batch of concrete cylinders from laboratory with a maximum size of 20mm). Therefore, good quality control of RCA was maintained in the production of the RAC used in this study. Further experimental data may be necessary to extend the applicability of Eq. (10) to other types of RAC. Indeed, in cases where RCA materials are obtained from unknown sources, the relationship between shear strength and the compressive strength and RCA replacement level can be different. For such cases, previous studies [1,7,10,11] suggest the use of reduction factors on existing code equations to conservatively predict the shear strength of RAC members.

In the following section, the shear stress predicted by Eq. (10) is compared against experimental values from actual tests.

## 5.2 Comparison of experimental shear stress and predictions

Figs. 13a-e show the relationships between shear stress and slip for specimens with different RCA replacement levels. The figures include the experimental results from the Z push-off specimens (LVDTs and DIC), results from the FEA analysis, as well as the results predicted by Eq. (10). The results show that increasing the level of replacement of RCA by 25%, 50%, 75% and 100%, the shear strength of concrete reduced by 4.3%, 9.1%, 12.8% and 17.3% respectively. Furthermore, a small stiffness reduction can be seen in the graph due to replacement of natural aggregates with RCA.

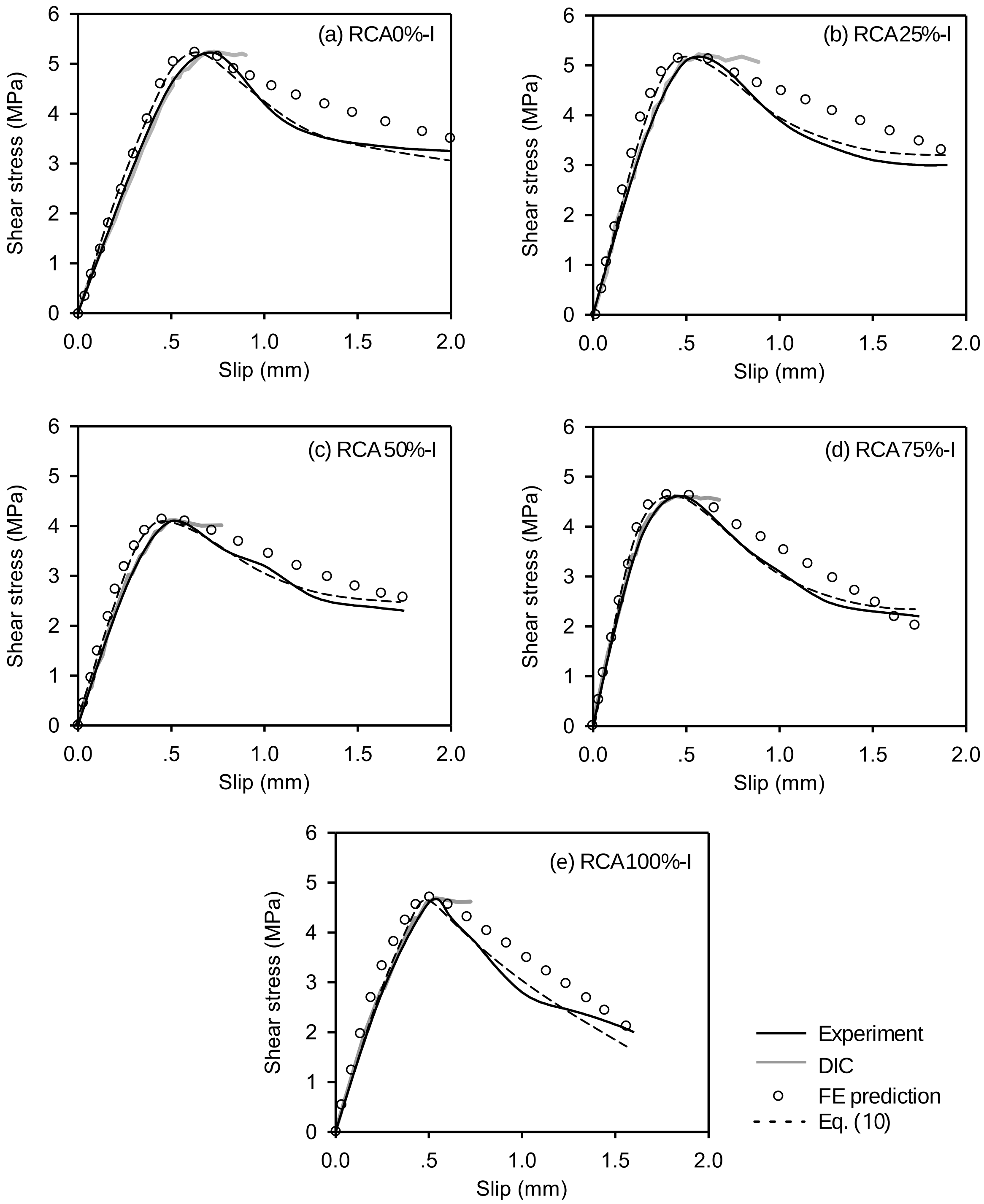


**Fig. 13.** Relationship between shear stress vs RCA replacement levels of (a) 0%, (b) 25%, (c) 50%, (d) 75%, and (e) 100% including experimental results, FEA results and predictions by Eq. (10).

Figs. 13a-e indicate that there is a good agreement between the different results. This suggests that the shear transfer mechanism in NAC and RAC is similar, and thus existing models can be calibrated to consider the different replacement levels of RCA in the concrete. The FE results showed that shear deformation along the cracked plane of Z-push off specimen under pure shear loading can be simulated and major cracks can be captured before the failure of specimen occurred. Likewise, Eq. (10) predicts accurately the shear stress and slip of the Z push-off specimens. However, further research is needed to validate these observations using different specimen geometries under shear loading. Moreover, further analysis of structures with other types, size, replacement levels and surface treatments of RAC should be investigated to confirm the findings presented in this study.

### 5.3 Model validation

The accuracy of the proposed Eq. (10) at predicting the shear strength of plain concrete with RCA is validated using tests carried out in this study and data available in the literature. Moreover, the shear stress models in ACI 318 for plain concrete and from past studies (Eqs. 1 and 2) are also considered including Eq. 10 and the maximum value of shear was picked and plotted. Fig. 14 shows the variation of the normalised shear stress ($\tau_{agg}/f_c$) with the RCA replacement level. It is shown that the predictions from ACI 318 give the most conservative results and are independent on the RCA replacement level. The normalized shear strength predicted by Walraven and Reinhardt (Eq. 1) and Li and Maekawa (Eq. (2)) increase with the RCA replacement level. However, Eq. (1) cannot predict well the test results presented in this study, whereas Eq. (2) cannot be applied if the RCA replacement level is 0 (i.e. to specimens made of normal concrete). Conversely, the proposed model (Eq. (10)) gives predictions better the shear stress provided by aggregate interlock of plain concrete at different RCA replacement levels.

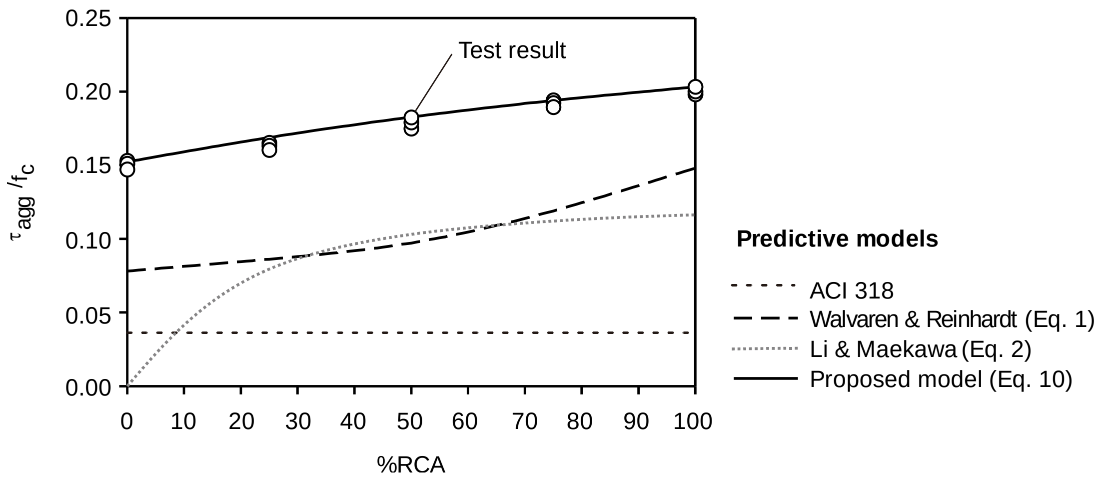

**Fig. 14.** Comparison of normalized shear strength vs with the RCA replacement level predicted by different shear equations.

To assess the accuracy of the proposed model at predicting the shear stress from other test results, 98 test data were compiled from the literature and from the tests presented in this study (see Appendix A). The results are sorted in groups and include the geometry of the Z-push off specimens, RCA replacement level, concrete strength, shear stress, crack width and slip. All of the specimens in this table were Z push-off specimens tested under direct shear loading arrangements.

The results in Appendix A indicate that existing empirical models (Eqs. (1) and (2)) do not predict well the test results and are characterised by high values of standard deviation (SD). For instance, Eq. (1) has a Prediction/Experiment ratio P/E=0.21 and a high SD=0.37, whereas Eq. (2) has a P/E =0.38 and a high SD=0.39. The ACI 318 empirical equation has P/E=0.15 and a SD=0.06 but gives reasonable safe predictions. It is also evident that Eq. (10) predicts better the test results with a P/E=0.83 and a SD=0.32. The high value of SD reflects the variation of RCA obtained from different sources.

Fig. 15 compares the predictions given by the new proposed model (Eq. (10)) and by Eqs. (1) and (2). The results show that the proposed model leads to more consistent and economic predictions compared to existing models. Accordingly, if no information about the crack width and slip is available (i.e. $w$=0, $\Delta$ =0), the shear stress can still be reasonably calculated using Eq. (10).

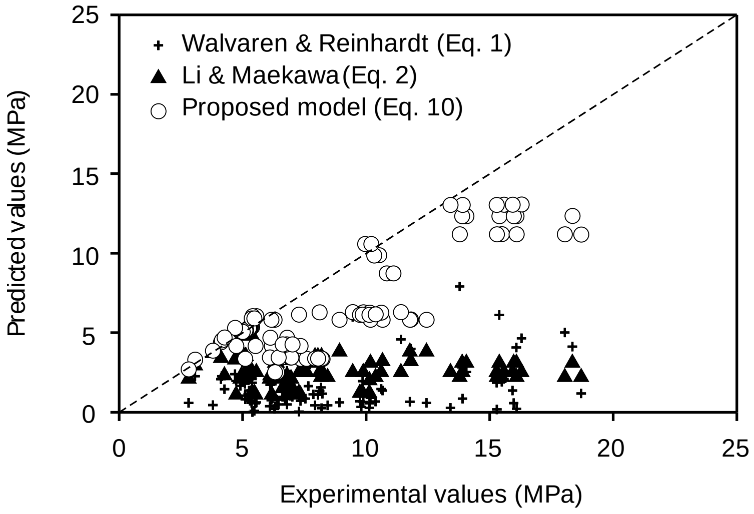


**Fig. 15.** Comparison of experimental values and different shear equations.

## 6. Conclusions

This article investigates experimentally and numerically the shear failure mechanism of Recycled Aggregate Concrete (RAC) specimens. Fifteen Z push-off type RAC specimens were first tested to examine the effect of different replacement levels of recycled concrete aggregate (fine and coarse at 0, 25%, 50%, 75% and 100%) on the shear strength of the specimens. The shear behaviour of the specimens was further examined using Digital Image Correlation analysis and nonlinear finite element analyses (FEA). A new equation to calculate the shear strength of specimens with different percentages of RAC is proposed. The equation adopts a fracture mechanics approach, and it explicitly includes the shear displacement and crack opening. From the results presented in this article, the following conclusions can be drawn:

1) The results from Z push-off specimesn tested in this study indicate that the replacement of natural aggregates with recycled concrete aggregates (RCAs) consistnetly reduces the shear strength of concrete. Such reduction is of 17.3% if 100% of the natural aggregates are replaced with fine and coarse RCAs.
2) Overall, the DIC and FEA predict well the shear stress–slip relationships obtained from the tested Z push-off specimens.
3) Whilst the normalised shear stress predicted by Walraven and Reinhardt and Li and Maekawa equations increase with the RCA replacement level, such equations can lead to inconsistent results. For instance, the the latter equation cannot be applied to specimens with an RCA replacement level of 0 (i.e. to specimens made of normal concrete).
4) Compared to existing models, the new semi-empirical equation calculates more accurately the shear strength of a dataset of 98 specimens with different percentages of RAC (Prediction/Experiment=0.83, SD=0.32). However, further experimental results are necessary to validate and extend the applicatbilty of the proposed equation to other types of concretes made with different types and amounts of RCAs.

## Acknowledgements

This research was funded by National Research Council of Thailand (NRCT5-RSA63019-04). This project was also supported by the Capacity Enhancement and Driving Strategies for Bilateral and Multilateral Cooperation for 2021 (Thailand and United Kingdom).

## References


1. M. Setkit, S. Leelatanon, T. Imjai, R. Garcia, S. Limkatanyu. Prediction of shear strength of reinforced recycled aggregate concrete beams without stirrups. Buildings 11 (2021) 402.
2. S. Leelatanon, T. Imjai, M. Setkit, R. Garcia, B. Kim. Punching shear capacity of recycled aggregate concrete slabs. Buildings 12 (2022) 1584.
3. M. Sogo, T. Sogabe, I. Maruyama, R. Sato, K. Kawai. Shear behavior of reinforced recycled concrete beams. In: International RILEM Conference on the Use of Recycled Materials in Buildings and Structures, Barcelona, Spain, 8–11 November 2004.
4. M. Etxeberria, A. Mari, E. Vázquez. Recycled aggregate concrete as structural material. Mater. Struct. 40 (2007) 529–541.
5. B. González-Fonteboa, F. Martínez-Abella. Shear strength of recycled concrete beams. Constr. Build. Mater. 21 (2007) 887–893.
6. A.M. Knaack, Y.C. Kurama, Behavior of reinforced concrete beams with recycled concrete coarse aggregates. J. Struct. Eng. 141 (2015) B4014009.
7. I. Ignjatović, S.B. Marinković, N. Tošić. Shear behaviour of recycled aggregate concrete beams with and without shear reinforcement. Eng. Struct. 141 (2017) 386–401.
8. M. Arezoumandi, A. Smith, J.S. Volz, K. Khayat. An experimental study on shear strength of reinforced concrete beams with 100% recycled concrete aggregate. Constr. Build. Mater. 53 (2014) 612–620.
9. M. Arezoumandi, J. Drury, J.S. Volz, K. Khayat. Effect of recycled concrete aggregate replacement level on shear strength of reinforced concrete beams. ACI Mater. J. 112 (2015) 559.
10. K. Rahal, Y. Alrefaei. Shear strength of longitudinally reinforced recycled aggregate concrete beams. Eng. Struct. 145 (2017) 273–282.
11. E.E. Etman, H.M. Afefy, A.T. Baraghith, S.A. Khedr. Improving the shear performance of reinforced concrete beams made of recycled coarse aggregate. Constr. Build. Mater. 185 (2018) 310–324.
12. S. Pradhan, S. Kumar, S.V. Barai. Shear performance of recycled aggregate concrete beams: an insight for design aspects. Constr. Build. Mater. 178 (2018) 593–611.
13. J. Xiao, H. Xie, Z. Yang. Shear transfer across a crack in recycled aggregate concrete. Cem. Concr. Res. 42 (2012) 700-709.
14. K.N. Rahal, W. Hassan. Shear strength of plain concrete made of recycled low-strength concrete aggregates and natural aggregates. Constr. Build. Mater. 311 (2021) 125317.
15. S. Ismail, M. Ramli. Engineering properties of treated recycled concrete aggregate (RCA) for structural applications. Constr. Build. Mater. 44 (2013) 464-476.

16. ACI. Building Code Requirements for Structural Concrete (ACI 318–14) and Commentary on Building Code Requirements for Structural Concrete (ACI 318R–14), ACI Committee 318, American Concrete Institute, Farmington Hills, MI, 2014.
17. E.C. Bentz, M.P. Collins, Development of the 2004 Canadian Standards Association (CSA) A23.3 Shear provisions for reinforced concrete. Can. J. Civ. Eng. 33 (2006) 521-534.
18. J. Xiao, W. Li, Y. Fan, X. Huang. An overview of study on recycled aggregate concrete in China (1996–2011). Constr. Build. Mater. 31, (2012) 364-383.
19. E. Cuenca, P. Serna. Shear behavior of Self-Compacting concrete and Fiber-Reinforced concrete push-off specimens. In Design, Production and Placement of Self-Consolidating Concrete: Proceedings of SCC2010, Montreal, Canada, September 26-29, (2010) 429-438.
20. J. Echegaray-Oviedo, J. Navarro-Gregori, E. Cuenca, P. Serna. Upgrading the push-off test to study the mechanisms of shear transfer in FRC elements. In Proceedings of the 8th International Conference on Fracture Mechanics of Concrete and Concrete Structures, FraMCoS (2013) 1012-1021.
21. W. Kaufmann, A. Amin, A. Beck, M. Lee. Shear transfer across cracks in steel fibre reinforced concrete. Eng. Struct. 186 (2019) 508-524.
22. J. Echegaray-Oviedo, J. Navarro-Gregori, E. Cuenca, P. Serna. Modified push-off test for analysing the shear behaviour of concrete cracks. Strain. 2017, 53(6).
23. B. Barragán, R. Gettu, L. Agulló, R. Zerbino. Shear failure of steel fiber-reinforced concrete based on push-off tests. ACI materials journal, 2006, 103(4), 251.
24. H.P.J. Taylor. Investigation of the forces carried across cracks in reinforced concrete beams in shear by interlock of aggregate. Technical Report No. TR 42.447. Cement and Concrete Research, Elmsford, NY (1970).
25. S.G. Millard, R. P. Johnson. Shear transfer in cracked reinforced concrete. Mag. Concr. Res. 37 (1985) 3-15.
26. J. Sagaseta, R. Vollum. Influence of aggregate fracture on shear transfer through cracks in reinforced concrete. Mag. Concr. Res. 63 (2011)119-137.
27. H. Jiang, Z. Fang, A. Liu, Y. Li, J. Feng. Interface shear behavior between high-strength precast girders and lightweight cast-in-place slabs. Constr. Build. Mater. 128 (2016) 449-460.
28. J.C. Walraven, H. W. Reinhardt. Theory and experiments on the mechanical behavior of cracks in plain and reinforced concrete subjected to shear loading. HERON, 26 (1A).
29. B. Li. Contact density model for stress transfer across cracks in concrete. Journal of the Faculty of Engineering, University of Tokyo. 1 (1989) 9-52.
30. BS EN 12390-3. Testing hardened concrete Part 3: Compressive strength of test specimens, British Standards Institution, London UK. (2019)

31. BS EN 12390–6. Testing hardened concrete Part 6: Tensile splitting strength of test specimens, British Standards Institution, London UK. (2020)
32. BS EN 12390–5. Testing hardened concrete Part 5: Flexural strength of test specimens. British Standards Institution, London UK. (2019)
33. BS EN 1992-1-1. Eurocode 2: Design of concrete structures, Part 1-1: General rules and rules for buildings. British Standards Institution, London UK. (2004)
34. B. Torres, F. B. Varona, F. J. Baeza, D. Bru, S. Ivorra. Study on retrofitted masonry elements under shear using digital image correlation. Sensors, 20 (2020) 2122.
35. J. Réthoré, F. Hild, S. Roux. Shear-band capturing using a multiscale extended digital image correlation technique. Comput. Methods Appl. Mech. Eng. 196 (2007) 5016-5030.
36. S. Jung, K.S. Kim. Knowledge-based prediction of shear strength of concrete beams without shear reinforcement. Eng. Struct. 30 (2008) 1515-1525.
37. P. Kanhakorn, W. Rerksamosorn, W. Rerksamosorn, N. Inmontien, T. Imjai, M. Setkit, S.Tippakdee, C. Wattanapanich. Estimation of shear behaviour for recycled aggregate concrete using digital image correlation (WU-DIC). Journal of KMUTNB, 33 (2022) 1-14.
38. B.L. Karihaloo, H.M. Abdalla, T. Imjai. A simple method for determining the true specific fracture energy of concrete. Mag. Concr. Res. 55 (2003) 471-481.
39. RILEM Committee FMC 50. Determination of the fracture energy of mortar and concrete by means of the three-point bend tests on notched beams. Mater. Struct. 18 (1985) 285–290.
40. X.R. Fu, S. Cen, C. F. Li, X. M. Chen. Analytical trial function method for development of new 8-node plane element based on the variational principle containing Airy stress function. Eng. Comput. (2010).
41. A.M. Tarantino. Thin hyperelastic sheets of compressible material: field equations, Airy stress function and an application in fracture mechanics. J. Elast. 44 (1996) 37-59.
42. O. Szachter, E. Katzav, M. Adda-Bedia, M. Moshe. Nonlinear extension of Kolosov-Muskhelishvili stress function formalism. arXiv preprint arXiv:2208 (2022) 13181.
43. H. Yoshihara. Mode II critical stress intensity factor of wood measured by the asymmetric four-point bending test of single-edge-notched specimen while considering an additional crack length. Holzforschung, 66 (2012) 989-992.
44. T.Y. Ko, J. Kemeny. Determination of Mode II stress intensity factor using short beam compression test. In: 4th Asian Rock Mechanics Symposium, Singapore (2006).
45. S.A. Waseem, B. Singh. An experimental study on shear capacity of interfaces in recycled aggregate concrete. Struct. Concr. 19 (2018) 230-245.
46. J. Xiao, H. Xie, Z. Yang. Shear transfer across a crack in recycled aggregate concrete. Cem. Concr. Res. 42 (2012) 700-709.

**Appendix A**. Comparison of shear stress of recycled aggregate concrete by different models and test results.

| Reference | No. | Sample ID | L (mm) | B (mm) | t (mm) | $A_v$ ($mm^2$) | %RCA | $f_c$ (MPa) | $\tau_{exp}$ (MPa) | $w_s$ (mm) | $\Delta_y$ (mm) | Predicted shear strength (MPa) | | | |
|---|---|---|---|---|---|---|---|---|---|---|---|---|---|---|---|
| | | | | | | | | | | | | Eq. (1) | Eq. (2) | ACI 318 | Eq. (10) |
| Results from this study | 1 | RCA0%-I | 500 | 200 | 100 | $4x10^4$ | 0 | 35.2 | 5.38 | 0.4 | 0.74 | 1.85 | 4.80 | 1.19 | 5.36 |
| | 2 | RCA0%-II | 500 | 200 | 100 | $4x10^4$ | 0 | 35.2 | 5.34 | 0.32 | 0.81 | 2.75 | 4.80 | 1.19 | 5.36 |
| | 3 | RCA0%-III | 500 | 200 | 100 | $4x10^4$ | 0 | 35.2 | 5.31 | 0.38 | 0.78 | 2.13 | 4.80 | 1.19 | 5.36 |
| | 4 | RCA25%-I | 500 | 200 | 100 | $4x10^4$ | 25 | 32.4 | 5.32 | 0.44 | 0.92 | 2.09 | 4.80 | 1.14 | 5.47 |
| | 5 | RCA25%-II | 500 | 200 | 100 | $4x10^4$ | 25 | 32.4 | 5.29 | 0.61 | 0.66 | 0.72 | 4.80 | 1.14 | 5.46 |
| | 6 | RCA25%-III | 500 | 200 | 100 | $4x10^4$ | 25 | 32.4 | 5.28 | 0.32 | 0.86 | 2.79 | 4.80 | 1.15 | 5.47 |
| | 7 | RCA50%-I | 500 | 200 | 100 | $4x10^4$ | 50 | 28.9 | 5.27 | 0.42 | 0.92 | 2.06 | 2.40 | 1.07 | 5.28 |
| | 8 | RCA50%-II | 500 | 200 | 100 | $4x10^4$ | 50 | 28.9 | 5.23 | 0.57 | 0.82 | 1.14 | 2.40 | 1.07 | 5.28 |
| | 9 | RCA50%-III | 500 | 200 | 100 | $4x10^4$ | 50 | 28.9 | 5.26 | 0.56 | 0.91 | 1.36 | 2.30 | 1.08 | 5.28 |
| | 10 | RCA75%-I | 500 | 200 | 100 | $4x10^4$ | 75 | 26.5 | 5.14 | 0.25 | 0.75 | 2.65 | 3.50 | 1.03 | 5.14 |
| | 11 | RCA75%-II | 500 | 200 | 100 | $4x10^4$ | 75 | 26.5 | 5.09 | 0.41 | 0.84 | 1.78 | 3.50 | 1.03 | 5.14 |
| | 12 | RCA75%-III | 500 | 200 | 100 | $4x10^4$ | 75 | 26.5 | 5.11 | 0.47 | 0.56 | 0.81 | 3.50 | 1.03 | 5.14 |
| | 13 | RCA100%-I | 500 | 200 | 100 | $4x10^4$ | 100 | 24.8 | 4.91 | 0.56 | 1.11 | 1.66 | 2.10 | 0.99 | 5.04 |
| | 14 | RCA100%-II | 500 | 200 | 100 | $4x10^4$ | 100 | 24.8 | 4.96 | 0.23 | 0.96 | 3.67 | 2.30 | 0.11 | 5.04 |
| | 15 | RCA100%-III | 500 | 200 | 100 | $4x10^4$ | 100 | 24.8 | 5.00 | 0.37 | 1.24 | 3.12 | 2.10 | 0.11 | 5.04 |
| Rahal and Hassan [14] | 16 | RAC0% | 320 | 150 | 150 | $1.73 x10^4$ | 0 | 40.6 | 4.69 | 0.46 | 0.95 | 2.39 | 3.30 | 1.27 | 6.19 |
| | 17 | RAC20% | 320 | 150 | 150 | $1.73 x10^4$ | 20 | 36.2 | 4.12 | 0.49 | 0.97 | 2.08 | 3.40 | 1.21 | 5.52 |
| | 18 | RAC50% | 320 | 150 | 150 | $1.73 x10^4$ | 50 | 37 | 4.16 | 0.53 | 1.11 | 2.27 | 5.04 | 1.22 | 5.65 |
| | 19 | RAC100% | 320 | 150 | 150 | $1.73 x10^4$ | 100 | 38 | 3.08 | 0.62 | 1.31 | 2.27 | 6.36 | 1.24 | 5.80 |
| Waseem and Singh [41] | 20 | N-00-0-A | 450 | 500 | 150 | $6.3 x10^4$ | 0 | 38.24 | 6.29 | 0.13 | 0.11 | 0.21 | 3.80 | 1.24 | 5.81 |
| | 21 | N-00-0-B | 450 | 500 | 150 | $6.3 x10^4$ | 0 | 38.24 | 6.16 | 0.1 | 0.14 | 0.76 | 3.80 | 1.24 | 5.81 |
| | 22 | N-00-2-A | 450 | 500 | 150 | $6.3 x10^4$ | 0 | 38.24 | 8.92 | 0.94 | 0.16 | 0.61 | 3.80 | 1.24 | 5.81 |
| | 23 | N-00-2-B | 450 | 500 | 150 | $6.3 x10^4$ | 0 | 38.24 | 10.66 | 0.42 | 0.61 | 1.36 | 3.20 | 1.24 | 5.81 |
| | 24 | N-00-3-A | 450 | 500 | 150 | $6.3 x10^4$ | 0 | 38.24 | 11.81 | 0.24 | 0.82 | 3.99 | 3.20 | 1.24 | 5.82 |
| | 25 | N-00-3-B | 450 | 500 | 150 | $6.3 x10^4$ | 0 | 38.24 | 10.17 | 0.42 | 0.48 | 0.89 | 3.10 | 1.24 | 5.81 |
| | 26 | N-00-4-A | 450 | 500 | 150 | $6.3 x10^4$ | 0 | 38.24 | 11.77 | 1.13 | 0.17 | 0.66 | 3.80 | 1.24 | 5.80 |
| | 27 | N-00-4-B | 450 | 500 | 150 | $6.3 x10^4$ | 0 | 38.24 | 12.44 | 1.14 | 0.25 | 0.59 | 3.80 | 1.24 | 5.80 |
| | 28 | N-50-0-A | 450 | 500 | 150 | $6.3 x10^4$ | 50 | 34.4 | 5.56 | 0.12 | 0.15 | 0.61 | 2.50 | 1.07 | 6.26 |
| | 29 | N-50-0-B | 450 | 500 | 150 | $6.3 x10^4$ | 50 | 34.4 | 5.4 | 0.18 | 0.11 | 0.01 | 2.50 | 1.07 | 6.26 |
| | 30 | N-50-2-A | 450 | 500 | 150 | $6.3 x10^4$ | 50 | 34.4 | 9.88 | 0.36 | 0.36 | 0.64 | 2.50 | 1.07 | 6.27 |

**Appendix A**. Comparison of shear stress of recycled aggregate concrete by different models and test results (contd.)

| Reference | No. | Sample ID | L (mm) | B (mm) | t (mm) | $A_v$ (mm$^2$) | %RCA | $f_c$ (MPa) | $\tau_{exp}$ (MPa) | $w_s$ (mm) | $\Delta_y$ (mm) | Predicted shear strength (MPa) | | | |
|---|---|---|---|---|---|---|---|---|---|---|---|---|---|---|---|
| | | | | | | | | | | | | Eq. (1) | Eq. (2) | ACI 318 | Eq. (10) |
| Waseem and Singh [41] | 31 | N-50-2-B | 450 | 500 | 150 | $6.3 \times 10^4$ | 50 | 34.4 | 8.11 | 0.32 | 0.49 | 1.85 | 4.80 | 1.19 | 5.36 |
| | 32 | N-50-3-A | 450 | 500 | 150 | $6.3 \times 10^4$ | 50 | 34.4 | 9.46 | 0.2 | 1.08 | 2.75 | 4.80 | 1.19 | 5.36 |
| | 33 | N-50-3-B | 450 | 500 | 150 | $6.3 \times 10^4$ | 50 | 34.4 | 10.61 | 0.19 | 0.34 | 2.13 | 4.80 | 1.19 | 5.36 |
| | 34 | N-50-4-A | 450 | 500 | 150 | $6.3 \times 10^4$ | 50 | 34.4 | 11.41 | 0.19 | 0.82 | 2.09 | 4.80 | 1.14 | 5.47 |
| | 35 | N-50-4-B | 450 | 500 | 150 | $6.3 \times 10^4$ | 50 | 34.4 | 10.14 | 0.85 | 0.13 | 0.72 | 4.80 | 1.14 | 5.46 |
| | 36 | N-100-0-A | 450 | 500 | 150 | $6.3 \times 10^4$ | 100 | 30.24 | 5.37 | 0.13 | 0.16 | 2.79 | 4.80 | 1.15 | 5.47 |
| | 37 | N-100-0-B | 450 | 500 | 150 | $6.3 \times 10^4$ | 100 | 30.24 | 5.47 | 0.12 | 0.09 | 2.06 | 2.40 | 1.07 | 5.28 |
| | 38 | N-100-2-A | 450 | 500 | 150 | $6.3 \times 10^4$ | 100 | 30.24 | 9.8 | 0.15 | 0.14 | 1.14 | 2.40 | 1.07 | 5.28 |
| | 39 | N-100-2-B | 450 | 500 | 150 | $6.3 \times 10^4$ | 100 | 30.24 | 7.28 | 0.36 | 0.2 | 1.36 | 2.30 | 1.08 | 5.28 |
| | 40 | N-100-3-A | 450 | 500 | 150 | $6.3 \times 10^4$ | 100 | 30.24 | 9.75 | 0.28 | 0.31 | 2.65 | 3.50 | 1.03 | 5.14 |
| | 41 | N-100-3-B | 450 | 500 | 150 | $6.3 \times 10^4$ | 100 | 30.24 | 9.86 | 0.2 | 0.46 | 1.78 | 3.50 | 1.03 | 5.14 |
| | 42 | N-100-4-A | 450 | 500 | 150 | $6.3 \times 10^4$ | 100 | 30.24 | 10.13 | 0.67 | 0.2 | 0.81 | 3.50 | 1.03 | 5.14 |
| | 43 | N-100-4-B | 450 | 500 | 150 | $6.3 \times 10^4$ | 100 | 30.24 | 10.38 | 0.47 | 0.49 | 1.66 | 2.10 | 0.99 | 5.04 |
| | 44 | H-00-0-A | 450 | 500 | 150 | $6.3 \times 10^4$ | 0 | 73.6 | 8.17 | 0.05 | 0.1 | 3.67 | 2.30 | 0.11 | 5.04 |
| | 45 | H-00-0-B | 450 | 500 | 150 | $6.3 \times 10^4$ | 0 | 73.6 | 8.44 | 0.07 | 0.08 | 3.12 | 2.10 | 0.11 | 5.04 |
| | 46 | H-00-2-A | 450 | 500 | 150 | $6.3 \times 10^4$ | 0 | 73.6 | 13.78 | 0.1 | 0.48 | 2.39 | 3.30 | 1.27 | 6.19 |
| | 47 | H-00-2-B | 450 | 500 | 150 | $6.3 \times 10^4$ | 0 | 73.6 | 15.49 | 0.23 | 0.33 | 2.08 | 3.40 | 1.21 | 5.52 |
| | 48 | H-00-3-A | 450 | 500 | 150 | $6.3 \times 10^4$ | 0 | 73.6 | 15.29 | 0.49 | 0.34 | 2.27 | 5.04 | 1.22 | 5.65 |
| | 49 | H-00-3-B | 450 | 500 | 150 | $6.3 \times 10^4$ | 0 | 73.6 | 18.04 | 0.12 | 0.38 | 2.27 | 6.36 | 1.24 | 5.80 |
| | 50 | H-00-4-A | 450 | 500 | 150 | $6.3 \times 10^4$ | 0 | 73.6 | 18.7 | 0.82 | 0.15 | 0.21 | 3.80 | 1.24 | 5.81 |
| | 51 | H-00-4-B | 450 | 500 | 150 | $6.3 \times 10^4$ | 0 | 73.6 | 16.09 | 0.44 | 0.31 | 0.76 | 3.80 | 1.24 | 5.81 |
| | 52 | H-50-0-A | 450 | 500 | 150 | $6.3 \times 10^4$ | 50 | 67.6 | 7.86 | 0.11 | 0.15 | 0.61 | 3.80 | 1.24 | 5.81 |
| | 53 | H-50-0-B | 450 | 500 | 150 | $6.3 \times 10^4$ | 50 | 67.6 | 7.66 | 0.06 | 0.12 | 1.36 | 3.20 | 1.24 | 5.81 |
| | 54 | H-50-2-A | 450 | 500 | 150 | $6.3 \times 10^4$ | 50 | 67.6 | 14.06 | 0.24 | 0.42 | 3.99 | 3.20 | 1.24 | 5.82 |
| | 55 | H-50-2-B | 450 | 500 | 150 | $6.3 \times 10^4$ | 50 | 67.6 | 13.88 | 0.34 | 0.61 | 0.89 | 3.10 | 1.24 | 5.81 |
| | 56 | H-50-3-A | 450 | 500 | 150 | $6.3 \times 10^4$ | 50 | 67.6 | 16.08 | 0.18 | 0.46 | 0.66 | 3.80 | 1.24 | 5.80 |
| | 57 | H-50-3-B | 450 | 500 | 150 | $6.3 \times 10^4$ | 50 | 67.6 | 15.39 | 0.16 | 0.58 | 0.59 | 3.80 | 1.24 | 5.80 |
| | 58 | H-50-4-A | 450 | 500 | 150 | $6.3 \times 10^4$ | 50 | 67.6 | 18.35 | 0.26 | 0.63 | 0.61 | 2.50 | 1.07 | 6.26 |
| | 59 | H-50-4-B | 450 | 500 | 150 | $6.3 \times 10^4$ | 50 | 67.6 | 15.97 | 0.46 | 0.39 | 0.01 | 2.50 | 1.07 | 6.26 |
| | 60 | H-100-0-A | 450 | 500 | 150 | $6.3 \times 10^4$ | 100 | 64.4 | 7.29 | 0.1 | 0.14 | 0.64 | 2.50 | 1.07 | 6.27 |

**Appendix A**. Comparison of shear stress of recycled aggregate concrete by different models and test results (contd.)

| Reference | No. | Sample ID | L (mm) | B (mm) | t (mm) | $A_v$ (mm$^2$) | %RCA | $f_c$ (MPa) | $\tau_{exp}$ (MPa) | $w_s$ (mm) | $\Delta_y$ (mm) | Predicted shear strength (MPa) | | | |
|---|---|---|---|---|---|---|---|---|---|---|---|---|---|---|---|
| | | | | | | | | | | | | Eq. (1) | Eq. (2) | ACI 318 | Eq. (10) |
| Waseem and Singh [42] | 61 | H-100-0-B | 450 | 500 | 150 | 6.3 x10$^4$ | 100 | 64.4 | 7.54 | 0.08 | 0.11 | 0.86 | 2.50 | 1.61 | 13.02 |
| | 62 | H-100-2-A | 450 | 500 | 150 | 6.3 x10$^4$ | 100 | 64.4 | 13.41 | 0.37 | 0.27 | 0.28 | 2.50 | 1.61 | 13.03 |
| | 63 | H-100-2-B | 450 | 500 | 150 | 6.3 x10$^4$ | 100 | 64.4 | 13.9 | 0.28 | 0.28 | 0.85 | 2.50 | 1.61 | 13.03 |
| | 64 | H-100-3-A | 450 | 500 | 150 | 6.3 x10$^4$ | 100 | 64.4 | 15.57 | 0.23 | 0.37 | 2.09 | 2.50 | 1.61 | 13.04 |
| | 65 | H-100-3-B | 450 | 500 | 150 | 6.3 x10$^4$ | 100 | 64.4 | 15.28 | 0.16 | 0.26 | 1.86 | 2.50 | 1.61 | 13.03 |
| | 66 | H-100-4-A | 450 | 500 | 150 | 6.3 x10$^4$ | 100 | 64.4 | 16.29 | 0.26 | 0.71 | 4.65 | 2.50 | 1.61 | 13.06 |
| | 67 | H-100-4-B | 450 | 500 | 150 | 6.3 x10$^4$ | 100 | 64.4 | 15.92 | 0.35 | 0.42 | 1.36 | 2.50 | 1.61 | 13.04 |
| Xiao et al. [46] | 68 | N-13 | 600 | 400 | 150 | 12 x10$^4$ | 0 | 22.0 | 5.10 | 0.44 | 0.65 | 1.03 | 2.50 | 0.94 | 3.35 |
| | 69 | N-14a | 600 | 400 | 150 | 12 x10$^4$ | 0 | 22.0 | 7.35 | 0.30 | 0.94 | 2.58 | 2.50 | 0.94 | 3.35 |
| | 70 | N-14b | 600 | 400 | 150 | 12 x10$^4$ | 0 | 22.0 | 7.59 | 0.29 | 0.98 | 2.79 | 2.50 | 0.94 | 3.35 |
| | 71 | N-14c | 600 | 400 | 150 | 12 x10$^4$ | 0 | 22.0 | 8.23 | 0.43 | 0.69 | 1.17 | 2.50 | 0.94 | 3.34 |
| | 72 | N-24 | 600 | 400 | 150 | 12 x10$^4$ | 30 | 24.2 | 6.21 | 0.59 | 0.76 | 0.87 | 3.70 | 0.98 | 4.15 |
| | 73 | N-32 | 600 | 400 | 150 | 12 x10$^4$ | 30 | 22.5 | 3.8 | 0.60 | 0.54 | 0.45 | 3.70 | 0.95 | 3.86 |
| | 74 | N-33 | 600 | 400 | 150 | 12 x10$^4$ | 30 | 22.5 | 6.8 | 0.32 | 0.99 | 2.61 | 3.70 | 0.95 | 3.87 |
| | 75 | N-34 | 600 | 400 | 150 | 12 x10$^4$ | 30 | 22.5 | 6.82 | 0.51 | 0.86 | 1.27 | 3.70 | 0.95 | 3.87 |
| | 76 | R-14a | 600 | 400 | 150 | 12 x10$^4$ | 30 | 14.6 | 6.39 | 0.54 | 0.73 | 0.78 | 3.10 | 0.76 | 2.51 |
| | 77 | R-14b | 600 | 400 | 150 | 12 x10$^4$ | 30 | 14.6 | 6.31 | 0.59 | 0.48 | 0.35 | 3.10 | 0.76 | 2.51 |
| | 78 | R-42 | 600 | 400 | 150 | 12 x10$^4$ | 100 | 20.5 | 4.74 | 0.24 | 0.65 | 1.97 | 1.10 | 0.91 | 4.15 |
| | 79 | R-43 | 600 | 400 | 150 | 12 x10$^4$ | 100 | 20.5 | 5.52 | 0.48 | 0.49 | 0.56 | 1.10 | 0.91 | 4.15 |
| | 80 | R-44a | 600 | 400 | 150 | 12 x10$^4$ | 100 | 20.5 | 7.34 | 0.46 | 0.54 | 0.71 | 1.10 | 0.91 | 4.15 |
| | 81 | R-44b | 600 | 400 | 150 | 12 x10$^4$ | 100 | 20.5 | 6.78 | 0.51 | 0.80 | 1.09 | 1.10 | 0.91 | 4.16 |
| | 82 | R-44c | 600 | 40 | 150 | 12 x10$^4$ | 100 | 20.5 | 6.18 | 0.31 | 0.73 | 1.76 | 1.10 | 0.91 | 4.16 |
| | 83 | R-52 | 600 | 400 | 150 | 12 x10$^4$ | 50 | 25.7 | 4.27 | 0.46 | 0.81 | 1.45 | 2.30 | 1.02 | 4.69 |
| | 84 | R-53 | 600 | 400 | 150 | 12 x10$^4$ | 50 | 25.7 | 6.12 | 0.21 | 0.47 | 1.72 | 2.30 | 1.02 | 4.68 |
| | 85 | R-54 | 600 | 400 | 150 | 12 x10$^4$ | 50 | 25.7 | 6.80 | 0.5 | 0.46 | 0.49 | 2.30 | 1.02 | 4.68 |
| | 86 | R30-64a | 600 | 400 | 150 | 12 x10$^4$ | 30 | 19.6 | 7.93 | 1.16 | 1.26 | 0.43 | 3.50 | 0.89 | 3.37 |
| | 87 | R30-64b | 600 | 400 | 150 | 12 x10$^4$ | 30 | 19.6 | 8.20 | 1.01 | 0.79 | 0.24 | 3.50 | 0.89 | 3.37 |
| | 88 | R30-64c | 600 | 400 | 150 | 12 x10$^4$ | 30 | 19.6 | 8.05 | 0.56 | 0.89 | 1.09 | 3.50 | 0.89 | 3.37 |
| | 89 | R50-14a | 600 | 400 | 150 | 12 x10$^4$ | 50 | 18.9 | 6.72 | 0.64 | 0.84 | 0.83 | 2.10 | 0.87 | 3.45 |
| | 90 | R50-14b | 600 | 400 | 150 | 12 x10$^4$ | 50 | 18.9 | 6.60 | 0.45 | 0.91 | 1.47 | 2.10 | 0.87 | 3.45 |

**Appendix A**. Comparison of shear stress of recycled aggregate concrete by different models and test results (cont.)

| Reference | No. | Sample ID | L (mm) | B (mm) | t (mm) | $A_v$ (mm$^2$) | %RCA | $f_c$ (MPa) | $\tau_{exp}$ (MPa) | $w_s$ (mm) | $\Delta_y$ (mm) | Predicted shear strength (MPa) Eq. (1) | Eq. (2) | ACI 318 | Eq. (10) |
|---|---|---|---|---|---|---|---|---|---|---|---|---|---|---|---|
| Xiao et al. [46] | 91 | R50-72 | 600 | 40 | 15 | 12 x10$^4$ | 50 | 18.8 | 2.82 | 0.94 | 1.10 | 0.59 | 2.10 | 0.87 | 3.40 |
| | 92 | R50-73 | 600 | 40 | 15 | 12 x10$^4$ | 50 | 18.8 | 6.1 | 0.85 | 0.76 | 0.38 | 2.10 | 0.87 | 3.43 |
| | 93 | R50-74a | 600 | 40 | 15 | 12 x10$^4$ | 50 | 18.8 | 6.93 | 0.52 | 0.80 | 1.03 | 2.10 | 0.87 | 3.43 |
| | 94 | R50-74b | 600 | 40 | 15 | 12 x10$^4$ | 50 | 18.8 | 6.97 | 0.38 | 0.82 | 1.56 | 2.10 | 0.87 | 3.43 |
| | 95 | R50-74c | 600 | 40 | 15 | 12 x10$^4$ | 50 | 18.8 | 6.45 | 0.80 | 0.79 | 0.48 | 2.10 | 0.87 | 3.44 |
| | 96 | R70-84a | 600 | 40 | 15 | 12 x10$^4$ | 70 | 22.2 | 6.78 | 0.46 | 0.66 | 0.99 | 1.60 | 0.94 | 4.25 |
| | 97 | R70-84b | 600 | 40 | 15 | 12 x10$^4$ | 70 | 22.2 | 6.62 | 0.74 | 1.07 | 0.97 | 1.50 | 0.94 | 4.26 |
| | 98 | R70-84c | 600 | 40 | 15 | 12 x10$^4$ | 70 | 22.2 | 7.02 | 0.68 | 0.97 | 0.97 | 1.50 | 0.94 | 4.26 |
| **Mean value (Prediction / Experiment)** | | | | | | | | | | | | **0.21** | **0.38** | **0.15** | **0.83** |
| **Standard deviation (Prediction / Experiment)** | | | | | | | | | | | | **0.37** | **0.39** | **0.06** | **0.32** |

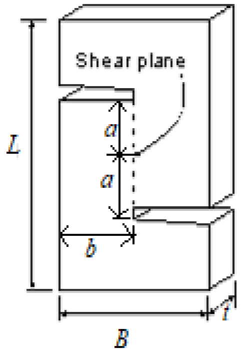


Note: B, L and t are the width, height sand thickness of a Z-push off specimen, shear plane is the planar where the shear load acting through the specimen, %RCA is the replacement ratio of recycled concrete aggregate to natural aggregate in the mix design, $f_c$ is the concrete compressive strength, $\tau_u$ is the maximum shear stress, $w_s$ and $\Delta_y$ are the crack width and slip measured at $\tau_u$.